Computational Field Visualization

Chris Johnson, Dean Brederson, Chuck Hansen, Milan Ikits,
Gordon Kindlmann, Yarden Livnat, Steve Parker,
David Weinstein, and Ross Whitaker

Scientific Computing and Imaging (SCI) Institute
School of Computing, University of Utah
Salt Lake City, UT 84112

July 16, 2001

1 Introduction

Today, scientists, engineers, and medical researchers routinely use computers to simulate complex physical phenomena. Such simulations present new challenges for computational scientists, including the need to effectively analyze and visualize complex three-dimensional data. As simulations become more complex and produce larger amounts of data, the effectiveness of utilizing such high resolution data will hinge upon the ability of human experts to interact with their data and extract useful information.

Here we describe recent work at the SCI Institute in large-scale scalar, vector, and tensor visualization techniques. We end with a discussion of ideas for the integration of techniques for creating computational multi-field visualizations.

2 Scalar Field Visualization

2.1 Direct Volume Rendering

Direct volume rendering is a method of displaying three-dimensional volumetric scalar data as a two-dimensional image. Direct volume rendering is probably the simplest way to visualize volume data. The individual values in the dataset are made visible by an assignment of optical properties, like color and opacity, which are then projected and composited to form an image. As a tool for scientific visualization, the appeal of direct volume rendering, in contrast to other rendering techniques such as isosurfacing or segmentation, is that no intermediate geometric information needs to be calculated, so the process maps from the dataset directly to an image.

It is typical to begin the design of a transfer function with the goal of visualizing the interface between two different materials in a volume dataset as a thin surface. User

defined transfer functions are frequently created as a mapping from a scalar field data value to opacity. To use this type of transfer function to visualize the interface between two materials, the user might set the function to be near zero over the domain of values except for a narrow spike centered on a single data value. This data value might initially be guessed at and then iteratively refined until the desired effect is achieved. More automatic methods for designing transfer functions for locating material interfaces have been explored.

The design of transfer functions using semi-automatic methods with abstracted levels of interaction becomes very important as the size of datasets, and hence required rendering time, grow with advances in measurement equipment and techniques. Also, where datasets and associated volume rendering methods are more complex (such as in vector or tensor visualization), methods for guiding the user towards useful parameter settings, based on information about the goal of the visualization, become a necessary part of generating informative scientific visualizations. Some of our initial work in this area is shown in Figure 1 [7].
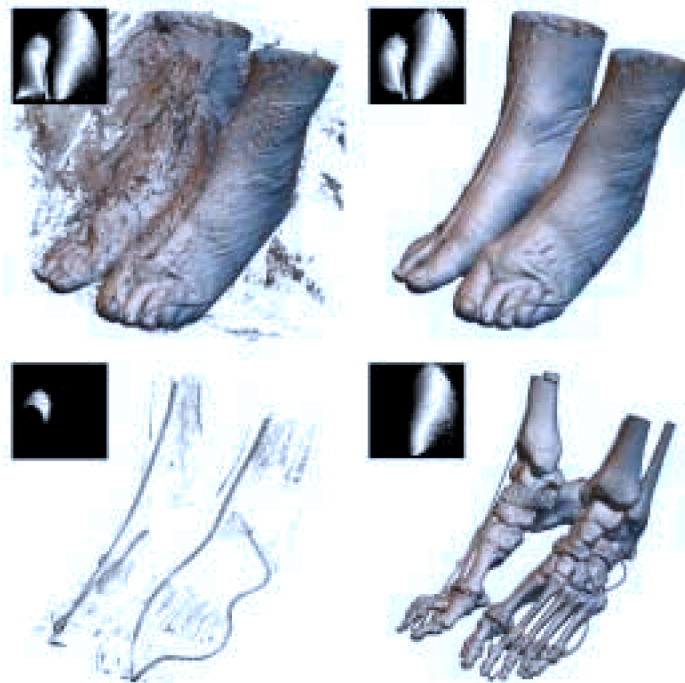

Figure 1: Manipulation of an automatically generated two-dimensional opacity function to selectively render different material boundaries: skin (upper right), bone (lower right), and the registration cord laced around the body prior to scanning (lower left).

In some cases volume visualization is more intimately tied to the imaging process.
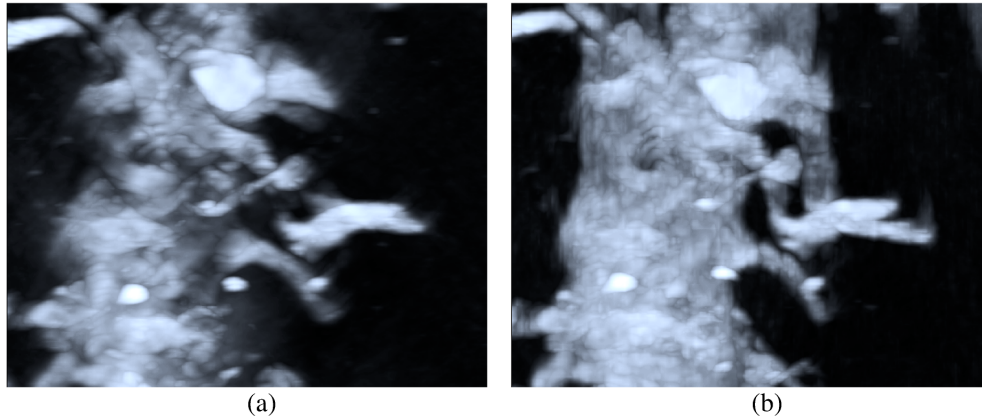

(a)   (b)

Figure 2: MIP renderings of EMT volumes: (a) from the raw data exhibits reconstruction artifacts that obsfuscate the boundaries of this spiney dendrite, and (b) from the original data including estimates of the missing views – brings to light a more coherent picture of dendrite structure.

For instance, in electron microscrope tomography (EMT) the set of projections (i.e. the sinogram) is incomplete, which results in reconstruction artifacts that adversely affect the quality of virtually any direct rendering or visualization strategy. Through a surface fitting process [3] we can estimate missing parts of the the sinogram and create better 3D reconstructions that are used for volume rendering or subsequent 3D segmentation.

2.2 Isosurface Extraction

Isosurface extraction is a powerful tool for investigating volumetric scalar fields. The position of an isosurface, as well as its relation to other neighboring isosurfaces, can provide clues to the underlying structure of the scalar field as seen in Figure 3. Scientists need the ability to change the isovalue dynamically in order to gain better insight into simulation results.

In recent years, researchers have created methods for accelerating the search phase for isosurface extraction [4, 5, 12, 14, 15] all of which have a complexity of $O(n)$. We introduced the *span space* [11] as a mean for mapping the search onto a two-dimension space. Using the span space, we proposed a *near optimal isosurface extraction* (NOISE) algorithm that has a time complexity of $0(\sqrt{n} + k)$, where k is the size of the isosurface. Cignoni *et al.* [2] employed another decomposition of the span space leading to a search method with optimal time complexity of $O(\log n + k)$, albeit with larger storage requirements.
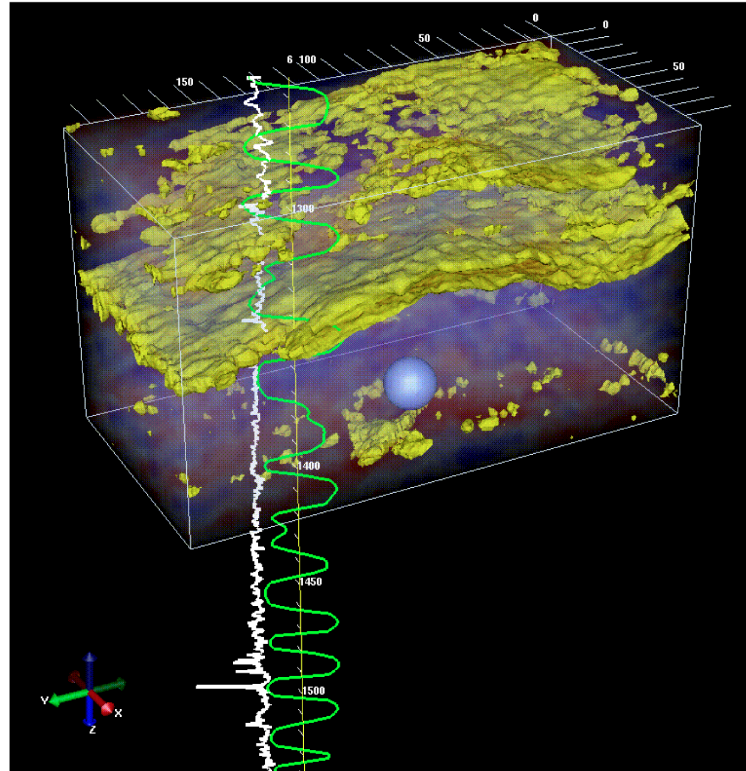
Figure 3: Imaging of seismic data. Two isosurfaces of a constant magnitude are shown embedded in a volume visualization of the data. A single trace and an SP-log curve at one of the wells are also shown.

Our recent research effort has concentrated on the *k* factor, *i.e.,* the size of the generated isosurface, in the complexity analysis. To this end, we have concentrated on view dependent extraction [10] and a ray-tracing approach that does not require the creation of an intermediate polygonal representation [13].

2.2.1 View Dependent Isosurface Extraction

View dependent isosurface extraction [10] is based on the observation that isosurfaces extracted from very large datasets tend to exhibit high depth complexity for two reasons. First, since the datasets are very large, the projection of individual cells tends to be sub-pixel. This leads to a large number of polygons, possibly non-overlapping, projecting onto individual pixels. Secondly, for some datasets, large sections of an isosurface are internal

4

and, thus, are occluded by other sections of the isosurface. These internal sections, common in medical datasets, cannot be seen from any direction unless the external isosurface is peeled away or cut off. Therefore, if one can extract just the visible portions of the isosurface, the number of rendered polygons will be reduced, and a faster algorithm will result.

We have created a view-dependent algorithm, see Figure 4, based on a hierarchical traversal of the data [10]. The algorithm exploits coherency in the object, value, and image spaces, as well as balancing the work between the hardware and the software. First, Wilhelms' and Van Gelder's algorithm is augmented by traversing down the octree in a front-to-back order in addition to pruning empty sub-trees based on the min-max values stored at the octree nodes. The second step employs coarse software visibility tests for each tree node which intersect the isosurface. The aim of these tests is to determine whether the tree node is hidden from the viewpoint by previously extracted sections of the isosurface (thus the requirement for a front-to-back traversal). Finally, the triangulation of the visible cells is forwarded to the graphics accelerator for rendering by the hardware. At this stage, the final and exact [partial-] visibility of the triangles is resolved.
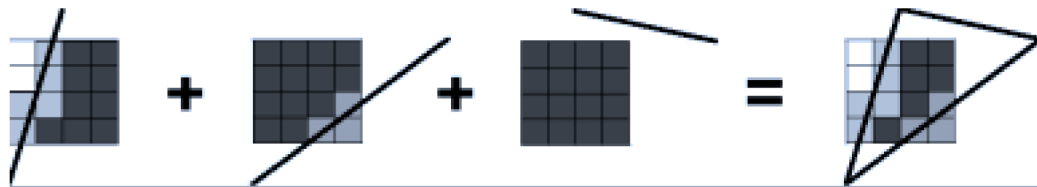

Figure 4: A view-dependent classification of cells and isoline

2.2.2 Real Time Ray Tracing of Isosurfaces

The previous methods extracted the geometry of an isosurface as a collection of triangles. We have created an alternative method that generates a single image of the isosurface from a given point of view [13]. No geometry is generated and thus a new image must be computed for each new point of view as well as each new isovalue. The image is generated using a conventional ray-tracing in which one or more rays are sent from the user point of view through each pixel of the screen and into the scene and show in Figure 5. A trilinear interpolation is used to approximate the isosurface inside each cell.

The parallel nature of a ray tracing maps well into the architecture of massive parallel computers. A 64 CPU Origin 2000 can generate images of an isosurface in interactive rate (about 10 frames per second) even for a large dataset (approximately 1GB). The complexity of a ray tracing isosurface extraction is only $O(m^2 \log n)$ where m^2 is the size of the screen, *i.e.,* it is linear with respect to the number of pixels in the final images, logarithmic with respect to the size of the data and does not depend on the size of the isosurface.

5

3   Vector Field Visualization

Visualizing 3D vector field data is a challenge because current methods cannot effectively convey large amounts of directional information without visual clutter. Researchers have developed a number of vector field visualization techniques using iconic representations, particle tracing methods, and stream constructions. These methods are useful for showing certain field characteristics, but inherently suffer from visual clutter when applied globally. We believe that interactive data exploration can be enhanced by the combined use of several interface modalities.

   Multimodal interfaces have been shown to increase user performance for a variety of tasks. We have been investigating the synergistic benefits of multimodal scientific visualization using an integrated, semi-immersive virtual environment, the Visual Haptic Workbench [1]. In this system, immersion is enhanced by head and hand tracking, haptic feedback, and additional audio cues.

   Since scientists would like to explore datasets over a wide range of scale, effective visualization must provide local inspection within a global context. Conventional visualization methods render the entire dataset and interactively restrict or highlight areas of interest. Our multimodal interface allows for a rich combination of local and global data rendering methods, which results in reduced visual clutter, enhanced spatial context, and the possibility for novel interaction paradigms (Figure 6).

4   Tensor Field Visualization

The simulation of a physical system often requires one to characterize the material property of the various media within the simulation domain, such as density, electrical or thermal conductivity, diffusivity etc. Further, one usually characterizes materials as to whether or not they are *homogeneous* and/or *isotropic*. Homogeneous materials are those whose properties do not depend on position. An isotropic material at any point has the same local properties in all directions, so a single scalar value is sufficient for the mathematical representation of those properties. If, however, materials have some preferred directions, they are called anisotropic. Examples of tensors are common in material science, engineering and physics. They include the conductivity σ_{ij} tensor, magnetic permutivity μ_{ij} and dielectric susceptibility ϵ *ij* tensors, and the diffusion tensor *D ij* [8].

   Diffusion Tensor MRI (DT-MRI) is an imaging modality that permits non-invasive measurement of tissue physical microstructure, via its influence on the local diffusion of water molecules. In regions where the tissue has a linear organization, such as in myelinated axon bundles comprising the white matter in the brain, or in muscle tissue, diffusion is preferentially directed along the fiber direction, and this phenomenon can be measured with DT-MRI. Getting meaningful images or models out of diffusion tensor data is very challenging, however, because each sample point has six degrees of freedom. Displaying this much information on a two-dimensional plane is possible [9], but extending this to three-dimensional tensor datasets is extremely hard because of the visual clutter caused when multiple projections of data representations overlap in screen space. One

6

approach is to use *judicious subsetting*, whereby only the tensor samples within certain essential structures are shown, producing both a global image of the main structure, as well as permitting local inspection of the tensor properties on the visible surface. This is the approach taken in Figure 7, which visualizes half of a diffusion tensor volume from a human brain. Using simple boxes as the glyph for tensor representation reduces polygon count tremendously, which helps for interaction with this dataset, consisting of over four million tensor data points.

5   Future: Computational Multi-Field Visualization

Computational field problems; such as computational fluid dynamics (CFD), electromagnetic field simulation, and weather modeling -- essentially any problems whose physics can be modeled effectively by ordinary and/or partial differential equations-- constitute the majority of computational science and engineering simulations. The output of such simulations might be a single field variable (such as pressure or velocity) or a combination of fields involving a number of scalar fields, vector fields, and/or tensor fields. As such, scientific visualization researchers have concentrated on effective ways to visualize large-scale computational fields. As noted above, most of our (and others) current and previous visualization research has focused on methods and techniques for visualizing a computational field variables (such as the extraction of a single scalar field variable as an isosurface). While single variable visualization often satisfies the needs of the user, it is clear that it would also be useful to be able to effectively visualize multiple fields simultaneously.

In our opinion, an area ripe for research is what we will term "multi-field" visualization in which a scientist could visualize combinations of the above fields in such a way as to see the *interactions* of the fields. The challenges for such multi-field visualizations are many: large-scale data, complicated geometries, heterogeneous and anisotropic material properties. Below we give two examples of multi-field visualization that illucidate the challenges of involved with providing a researcher with intuitive and useful visual feedback [6].

In Figure 8, we give a simple example of multi-field visualization from the simulation of electric current flow within an anisotropic media. The sample volume has Dirichlet (± 1 volts) boundary conditions on the opposite sides of the cube (orthogonal to the plane of view) and Neumann zero flux boundary conditions on all other sides. The media is described by a single conductivity tensor with all non-zero elements. The result is very unintuitive: the isosurfaces are no longer parallel to the sides of the cube and current lines are not orthogonal to these isosurfaces. Electric field lines will still be orthogonal to the isosurfaces, but will not be parallel to the sides of the cube.

In another example of multi-field visualization, Figure 9, we show the results of a large-scale finite element simulation of the distribution of electric current flow and voltage within an inhomogeneous model of the human head and brain. The image shows a combination of an isovoltage surface and streamlines of current flow within the context of the magnetic resonance image scans and geometric head model.

UU IR Author Manuscript

We are continuing our research on effective visualization techniques for such multi-field simulations.

6 Acknowledgments

UU IR Author Manuscript

References

[1] J.D. Brederson, M. Ikits, C.R. Johnson, C.D. Hansen, and J.M. Hollerbach. The visual haptic workbench. In *Proceedings of the Fifth PHANToM Users Group Workshop*, Aspen, CO, October 2000.

[2] P. Cignoni, C. Montani, E. Puppo, and R. Scopigno. Optimal isosurface extraction from irregular volume data. In *Proceedings of IEEE 1996 Symposium on Volume Visualization*. ACM Press, 1996.

[3] V. Elangovan and R. Whitaker. From sinograms to surfaces: A direct approach to segmenting tomographic data. In *Medical Image Computing and Computer-Assisted Intervention*.

[4] R.S. Gallagher. Span filter: An optimization scheme for volume visualization of large finite element models. In *Proceedings of Visualization '91*, pages 68--75. IEEE Computer Society Press, Los Alamitos, CA, 1991.

[5] T. Itoh, Y. Yamaguchi, and K. Koyyamada. Volume thining for automatic isosurface propagation. In *Visualization '96*, pages 303--310. IEEE Computer Society Press, Los Alamitos, CA, 1996.

[6] C.R. Johnson, Y. Livnat, L. Zhukov, D. Hart, and G. Kindlmann. Computational field visualization. In B. Engquist and W. Schmid, editors, *Mathematics Unlimited -- 2001 and Beyond*}, volume~2, pages 605--630. 2001.

[7] G. Kindlmann and J. Durkin. Semi-automatic generation of transfer functions for direct volume rendering. In *IEEE Symposium on Volume Visualization*, pages 79--86. IEEE Press, 1998.

[8] G.L. Kindlmann and D.M. Weinstein. Strategies for direct volume rendering of diffusion tensor fields. *IEEE Trans. Visualization and Computer Graphics*, 6(2):124--138, 2000.

[9] David H. Laidlaw, Eric T. Ahrens, David Kremers, Matthew J. Avalos, Russell E. Jacobs, and Carol Readhead. Visualizing Diffusion Tensor Images of the Mouse Spinal Cord. In *IEEE Visualization98*, pages 127--134, 1998.

[10] Y. Livnat and C. Hansen. View dependent isosurface extraction. In *Visualization '98*, pages 175--180. ACM Press, October 1998.

[11] Y. Livnat, H.W. Shen, and C.R. Johnson. A near optimal isosurface extraction algorithm using the span space. *IEEE Transaction on Visualization and Computer Graphics*, 2(1), March 1996.

[12] J.S. Painter, P. Bunge, and Y. Livnat. Case study: Mantle convection visualization on the cray t3d. In *Visualization '96*, pages 409--412. IEEE Computer Society Press, Los Alamitos, CA, 1996.

[13] S. Parker, P. Shirley, Y. Livnat, C. Hansen, and P. Sloan. Interactive ray tracing for isosurface rendering. In *Visualization '98*, pages 233--238. ACM Press, October 1998.

[14] H Shen, C. D. Hansen, Y Livnat, and C.R. Johnson. Isosurfacing in span space with utmost efficiency (ISSUE). In *Proceedings of Visualization '96*, pages 287--294. IEEE Computer Society Press, 1996.

[15] H.W. Shen and C.R. Johnson. Sweeping simplices: {A} fast isosurface extraction algorithm for unstructure grids. In *Proceedings of Visualization '95*. IEEE Computer Society Press, Los Alamitos, CA, 1995.

9

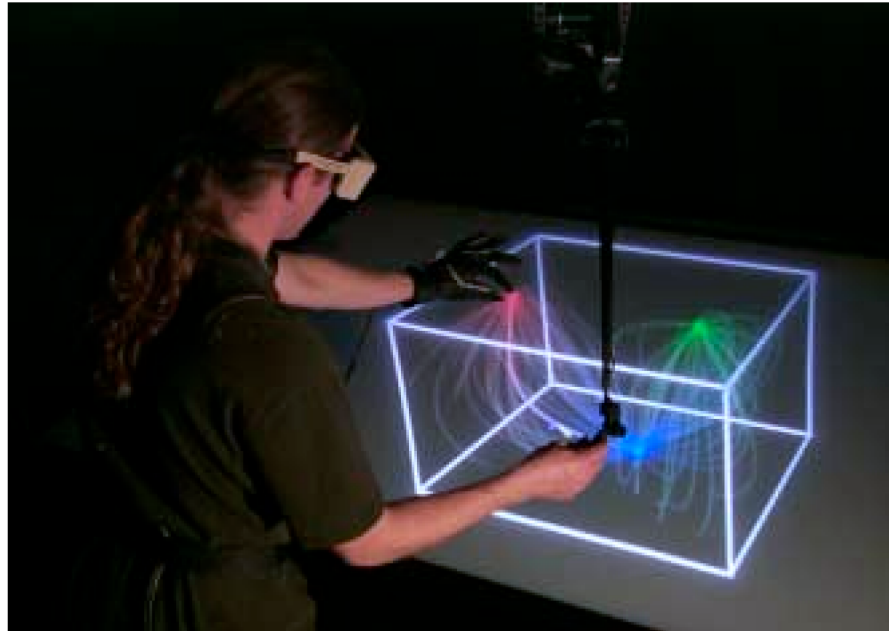Figure 5: Ray tracings of the bone and skin isosurfaces of the Visible Woman.

Figure 6: Exploring an electrostatic charge field on the Visual Haptic Workbench. Streamlines show the global structure of the field, colored by proximity to the sources (red and green spheres) and the sink (blue sphere). The streamballs are obtained by local advection from the interaction point, represented by the purple proxy and yellow force vector to the left of the PHANToM stylus.
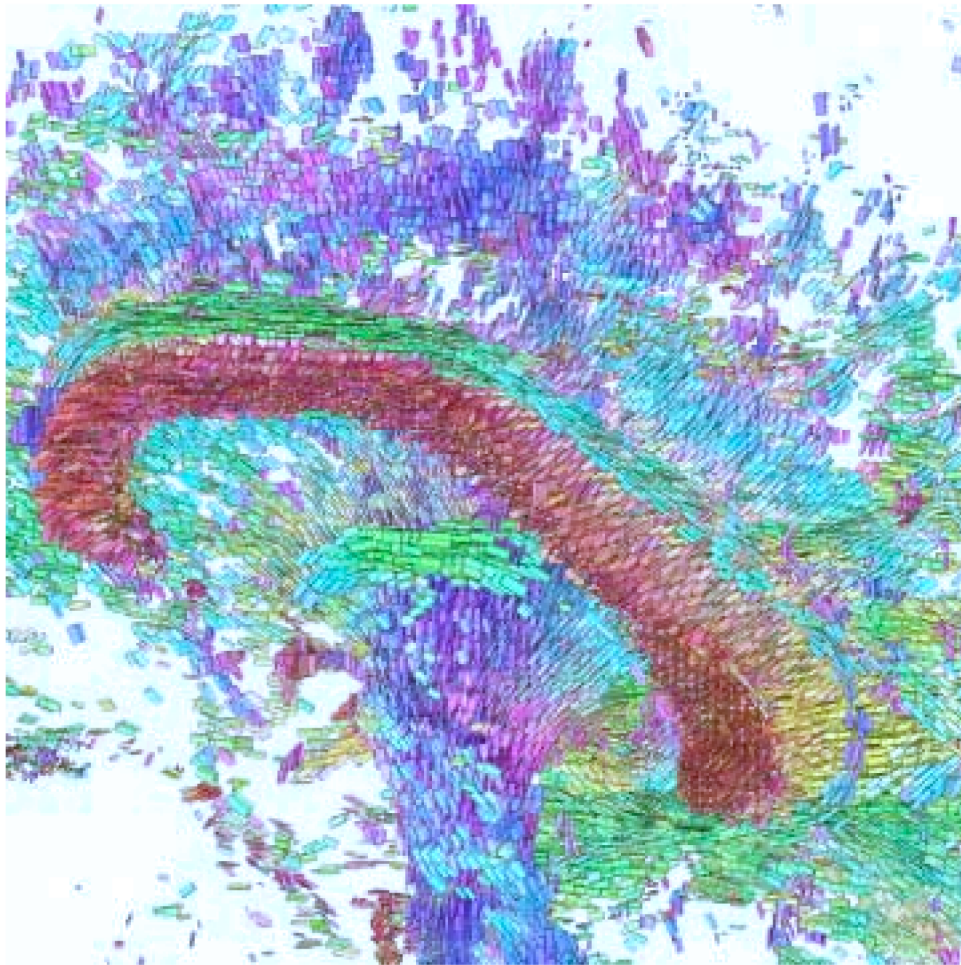
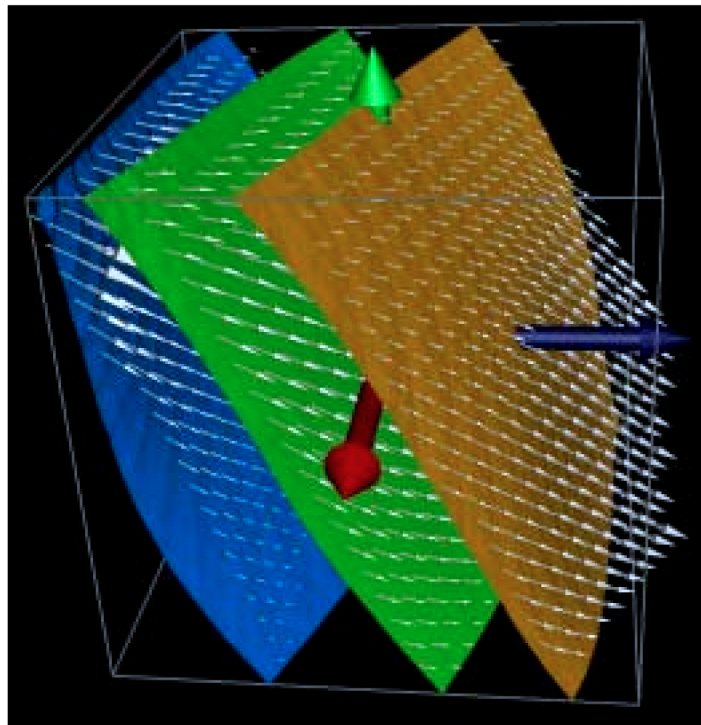Figure 7: Visualization of a DT-MRI of a section of the brain using box glyphs.

Figure 8: Electric current flow within an anisostropic media

Figure 9: Electric current flow within the brain due to a localized source.